Available online at www.sciencedirect.com

ScienceDirect

Physics Procedia 56 (2014) 211 – 219

Physics Procedia

8th International Conference on Photonic Technologies LANE 2014

Design of a model-based controller with temperature feedback for laser cladding

Wim Devesse[a,*], Dieter De Baere[a], Patrick Guillaume[a]

[a]*Vrije Universiteit Brussel, Acoustics and Vibration Research Group, Pleinlaan 2, B-1050 Brussels, Belgium*

Abstract

Laser cladding, also known as direct metal deposition, is an additive manufacturing technique for the production of freeform metallic parts. High quality parts can be created with the use of feedback control systems which stabilize the melt pool during the cladding process. Current laser cladding control systems are based on low order, empirical models of the process, which have low dynamic accuracy and limit the performance that can be achieved. In this paper, a control system based on a physical heat conduction model of the melt pool dynamics is presented. The control structure consists of a static linear state feedback control law designed using pole placement and combined with a PI controller. The controller is able to regulate the melt pool size by modulating the laser power using a number of surface temperature measurements as the feedback signal. Simulation results using a detailed finite element model show that the controller has good tracking behavior and disturbance rejection properties.

Peer-review under responsibility of the Bayerisches Laserzentrum GmbH

Keywords: Additive manufacturing; Feedback control; Laser cladding; Linear state feedback; Temperature control

1. Introduction

Additive manufacturing is an emerging technology that can be used for the production of freeform metallic parts. A promising additive manufacturing technique is laser cladding, also known as direct metal deposition (Toyserkani et al., 2005). The technique is being increasingly used for the creation of prototypes and more recently also for final part production. In the laser cladding process a high-power laser beam is focused on the surface of a solid metallic workpiece, locally heating the material and creating a melt pool. Metallic powder is blown into this melt pool where it mixes with the molten substrate material. As the nozzle is moving, the melt pool solidifies and a track of solid material (a clad) is formed.

In order to produce parts with high quality and precision, current laser cladding systems require careful tuning of the operational parameters such as the laser power and nozzle speed. These settings are then typically kept constant during the complete cladding process. However, variations in e.g. the geometry of the part can lead to overheating which negatively influences the resulting part quality. A lot of the research on laser cladding is therefore directed towards the control of the laser cladding process by using automatic feedback mechanisms.

* Corresponding author. Tel.: +32-485-545-913 .

E-mail address: Wim.Devesse@vub.ac.be

Peer-review under responsibility of the Bayerisches Laserzentrum GmbH

doi:10.1016/j.phpro.2014.08.165

Nomenclature

Latin symbols

Δh	specific latent heat of fusion [J/kg]
ΔT	temperature mesh spacing [K]
A	absorption coefficient [-]
A_c, B_c	continuous time system matrices
A_d, B_d	discrete time system matrices
C_p	specific heat [J/(kg·K)]
K, K_0	state feedback controller gains
K_p, K_i	PI controller gains
k	thermal conductivity [W/(m·K)]
L	characteristic length [m]
N	number of isotherms [-]
P	laser power [W]
p_i	closed loop system poles
r	radial coordinate [m]
S	characteristic time constant [s]
T	temperature [K]
t	time [s]
T_0	ambient temperature [K]
T_m	melting temperature [K]
$T_{\max}$	maximum isotherm temperature [K]
T_r	rise time [s]
T_s	sampling time [s]
U	laser speed [m/s]
u	system input
u_0	linearization point for system input
$\boldsymbol{x}$	system state vector
$\boldsymbol{x}_0$	linearization point for system state vector
x_m^{ref}	reference melt pool boundary position [m]

Greek symbols

α	thermal diffusivity [m^2/s]
β	thermal expansion coefficient [K^{-1}]
μ	dynamic viscosity [kg/(m·s)]
ρ	density [kg/m^3]
σ_i	open loop system poles
τ_i^+, τ_i^-	open loop system zeros
ξ, η, ζ	Cartesian coordinates [m]

The feedback control systems that can be found in the literature typically adapt the laser power based on real-time information of the melt pool temperature and size, obtained using e.g. a pyrometer or a camera based image recognition system. In these applications, the thermal dynamics of the laser cladding process are commonly approximated as a first or second order transfer function in the frequency domain and can be obtained experimentally (Fathi et al., 2007; Hofman et al., 2012; Salehi and Brandt, 2006). Such a model can be used to set the parameters of a Proportional-Integral-Derivative (PID) controller (Toyserkani et al., 2005; Fathi et al., 2007; Hofman et al., 2012; Salehi and Brandt, 2006; Doumanidis and Kwak, 2001; Bi et al., 2006) or to design a Model-Predictive Control (MPC) law (Song et al., 2012). While the use of these feedback control systems has been shown to result in an increased geometrical accuracy of the cladded parts, their performance is limited by the accuracy of the experimentally identified models.

Recently, a high order time-varying nonlinear state space model of the thermal dynamics in the melt pool during laser cladding was derived, which allows the development of more advanced control systems (Devesse et al., 2014). The model predicts the growth/decline of the melt pool as a function of the temperature distribution at the surface of the workpiece. Based on this model, a broad range of linear and nonlinear controllers can be designed for regulating the melt pool size using a number of surface temperature measurements as the feedback signal. In this paper, the state space model derived by Devesse is linearized around a fixed linearization point and used to design a linear state feedback controller which modifies the laser power using a number of temperature measurements. In order to improve its disturbance rejection properties, the controller is embedded in a PI control loop. The presented system gives an indication of the performance that can be achieved with a controller based on this high order dynamic thermal model.

The paper starts by presenting the dynamic thermal melt pool model as derived by Devesse. This model is then linearized and discretized in space so that it can be used to design a linear state feedback and PI controller in Section 3. The performance of the control system is evaluated using a number of simulations in Section 4. Final remarks and conclusions are given in Section 5.

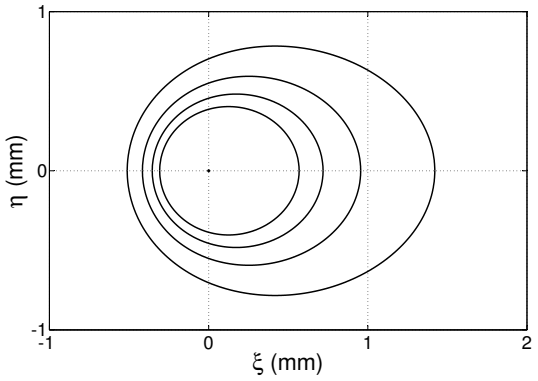

Fig. 1. Steady-state isotherms for $L = 1$ mm.

2. Physical model

In this section a model for laser cladding is presented based on the heat conduction equation in the workpiece. The model is a state space description of the thermal dynamics of the workpiece with the states equal to a set of isotherm positions. The model is subsequently linearized and discretized in time.

2.1. Heat conduction equation

Consider the problem of heating a semi-infinite workpiece ($\zeta \geq 0$) with a point source that is fixed in the origin. The workpiece has homogeneous material properties and moves with a constant speed U. If the direction of the workpiece is chosen as the positive ξ direction, the heat conduction equation can be written in the Cartesian coordinates ξ, η, ζ as follows (Dowden, 2001):

$$\frac{\partial T}{\partial t} = \alpha\left(\frac{\partial^2 T}{\partial \xi^2} + \frac{\partial^2 T}{\partial \eta^2} + \frac{\partial^2 T}{\partial \zeta^2}\right) - U\frac{\partial T}{\partial \xi} \tag{1}$$

where T is the temperature and α the thermal diffusivity, defined as $\alpha = k/(\rho C_p)$ with k the thermal conductivity, ρ the density of the material and C_p the specific heat. The steady-state solution of equation (1) is well-known and given by Rosenthal (1946):

$$T(\xi, \eta, \zeta) = T_0 + \frac{AP}{2\pi k r}\exp\left(\frac{\xi - r}{L}\right) \tag{2}$$

with $r = \sqrt{\xi^2 + \eta^2 + \zeta^2}$, P the laser power, A the absorption coefficient and T_0 the ambient temperature. The steady-state isotherms at the surface of the workpiece have an elliptical shape with an aspect ratio that depends on the characteristic length $L = 2\alpha/U$. The isotherms are shown in Figure 1 for $L = 1$ mm.

A change of variables can be applied to the heat conduction equation (1) to obtain a one-dimensional isotherm migration equation in η (Devesse et al., 2014). The equation is only valid on the η axis ($\xi = \zeta = 0$) and is given by:

$$\frac{\partial \eta}{\partial t} = \alpha\eta^2\frac{\partial}{\partial T}\left(\frac{1}{\eta^2}\frac{\partial \eta}{\partial T}\right)\left(\frac{\partial \eta}{\partial T}\right)^{-2} + \frac{T - T_0}{S}\frac{\partial \eta}{\partial T} \tag{3}$$

with $S = 4\alpha/U^2$ a characteristic time constant. Equation (3) describes the dynamics of the η-position of an isotherm with fixed temperature T. If this temperature is chosen to be equal to the melting temperature T_m, equation (3) gives the dynamics of the melt pool boundary position on the η axis, denoted by η_m. Assuming that the isotherms remain ellipsoidal in transient regime, the width, length and depth of the melt pool can then be derived from the value of η_m using Rosenthal's solution (2).

2.2. State space representation

Equation (3) can be discretized in space using a one-dimensional mesh of N temperatures T_i ($i = 1, \ldots, N$) with maximum temperature $T_1 = T_{\max}$ and equal spacing $\Delta T = (T_{\max} - T_0)/N$. The temperature values are defined as $T_i = T_0 + (N - i + 1)\Delta T$ and the position of each temperature is given by $\eta_i = \eta(T_i)$. A finite difference formulation of equation (3) on this mesh, including the appropriate boundary conditions of a point heat source with power P in the origin and letting $T(\eta = \infty) = T_0$, can then be derived:

$$\dot{\eta}_1 = -\frac{2\alpha}{\eta_1}\left(\frac{\eta_2}{\eta_2 - \eta_1}\right) + \frac{APe^{-\eta_1/L}}{\pi\rho C_p \Delta T \eta_1^2}\left(1 + \frac{\eta_1}{L}\right) - \frac{T_{\max} - T_0}{S\Delta T}(\eta_2 - \eta_1) \tag{4}$$

$$\dot{\eta}_i = -\frac{\alpha}{\eta_i}\left(\frac{\eta_{i+1}}{\eta_{i+1} - \eta_i} - \frac{\eta_{i-1}}{\eta_i - \eta_{i-1}}\right) - \frac{T_i - T_0}{2S\Delta T}(\eta_{i+1} - \eta_{i-1}) \qquad (i = 2, \ldots, N-1) \tag{5}$$

$$\dot{\eta}_N = -\frac{\alpha}{\eta_N}\left(\frac{\eta_N - 2\eta_{N-1}}{\eta_N - \eta_{N-1}}\right) - \frac{\eta_N - \eta_{N-1}}{S} \tag{6}$$

This system of equations is shown by Devesse et al. (2014) to converge to the actual solution for $N \to \infty$ and $T_{\max} \to \infty$.

Note that the equations (4) - (6) are a nonlinear state space description of the thermal dynamics of the workpiece with the states equal to a set of isotherm positions. Introducing a state vector $\boldsymbol{x} = (\eta_1, \ldots, \eta_N)^T$ and input $u = P$ we can write (4) - (6) more compactly as:

$$\dot{\boldsymbol{x}} = \boldsymbol{f}(\boldsymbol{x}, u) \tag{7}$$

where the vector-valued function $\boldsymbol{f}$ is given by the right-hand side of equations (4) - (6). The state space system (7) can be linearized around a linearization point $\boldsymbol{x}_0$, u_0 by introducing the Jacobian matrices $A_c \in \mathbb{R}^{N\times N}$ and $B_c \in \mathbb{R}^{N\times 1}$:

$$(A_c)_{ij} = \left.\frac{\partial f_i}{\partial x_j}\right|_{\substack{\boldsymbol{x}=\boldsymbol{x}_0 \\ u=u_0}}, \quad (B_c)_i = \left.\frac{\partial f_i}{\partial u}\right|_{\substack{\boldsymbol{x}=\boldsymbol{x}_0 \\ u=u_0}} \tag{8}$$

We can then write:

$$\dot{\boldsymbol{x}} = A_c\boldsymbol{x} + B_c u \tag{9}$$

where the state vector $\boldsymbol{x}$ and input u are redefined to contain the deviations from the linearization point $\boldsymbol{x}_0$, u_0. Note that due to the structure of equations (4) - (6), A_c is a tridiagonal matrix with negative real eigenvalues.

The system (9) can be discretized in time, assuming a Zero Order Hold (ZOH) for the input. Sampling this system with a constant sampling time T_s, the discrete time system is given by:

$$\dot{\boldsymbol{x}} = A_d\boldsymbol{x} + B_d u \tag{10}$$

with $A_d = \exp(A_c T_s)$ and $B_d = \int_{t'=0}^{T_s} \exp(A_c t')B_c \cdot dt'$.

3. Controller design

The state space system (10) can be used to design a control system for the laser cladding process. The presented controller consists of a combined linear state feedback and PI control and will be derived in this section.

3.1. Control structure

The goal of this section is to design a control system that is able to regulate the melt pool width by adjusting the power of the laser beam, given a number of temperature measurements along the positive η axis (that is, directly below the nozzle). Assuming that a mesh of N temperatures is defined as in Section 2.2, the actual positions of these

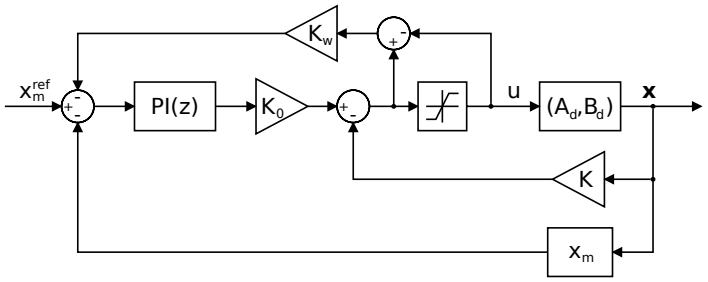

Fig. 2. Control structure.

temperatures can be determined from the temperature measurements using linear interpolation. If the temperature with index m is chosen as the melting temperature T_m, its position η_m can then be used to track the boundary of the melt pool on the η axis.

The measured (interpolated) isotherm positions η_i can be used to construct a state vector $\boldsymbol{x}$ by subtracting the linearization point $\boldsymbol{x}_0$:

$$\boldsymbol{x} = (\eta_1, \ldots, \eta_m, \ldots, \eta_N)^T - \boldsymbol{x}_0 \tag{11}$$

The dynamics of the state vector are given by equation (10). It can easily be checked that this system is reachable[1], so that a state feedback controller can be designed which is able to make the state value x_m follow a given reference x_m^{ref}. In order to remove a potential steady-state error and improve the disturbance rejection properties of the controller, a PI controller is placed in front of this system and enclosed in a second feedback loop. A back-calculation scheme is used to avoid integral windup. The complete control structure is shown in Figure 2, in which the (A_d,B_d) block represents the linear system (10) with an input that is saturated, K and K_0 are the state feedback gains, PI(z) is a discrete time PI controller, K_w is the anti-windup gain and the x_m block extracts the state x_m from the state vector $\boldsymbol{x}$. The values of the state feedback and anti-windup gains and the PI controller will be derived next.

3.2. Linear state feedback

The linear system (10) has N poles σ_i ($i = 1, \ldots, N$), which are all real and stable. In addition to these poles, the transfer function between the input u and the state x_m contains $(N-1)$ real zeros. $(m-1)$ of these zeros are negative and are introduced due to the sampling of the continuous time system (9). They will be denoted by τ_i^-. The other $(N-m)$ zeros, denoted by τ_i^+, are positive and lie inside the unit circle. The locations of the poles and zeros are shown in the left plot of Figure 3 for $N = 6$, $T_{\max} = 2120$ °C, with the material parameter values given in Table A.1 and with a sampling time of $T_s = 1$ ms.

A pole-zero cancellation can be performed by choosing $(N-m)$ closed loop poles equal to τ_i^+. The closed loop system response is then mainly determined by σ_m, the largest pole that is left. If this pole is set equal to

$$\sigma_m^* = e^{-T_s/T_r} \tag{12}$$

the rise time of the melting isotherm will be approximately equal to the specified value of T_r. In summary, the desired closed loop poles, denoted by p_i, are given by:

$$p_i = \begin{cases} \sigma_i & i = 1, \ldots, m-1 \\ \sigma_m^* & i = m \\ \tau_{i-m}^+ & i = m+1, \ldots, N \end{cases} \tag{13}$$

The closed loop poles and zeros are shown in the right plot of Figure 3 for $T_r = 10$ ms.

[1] Observing that A_c is a tridiagonal matrix and all the elements of B_c are zero except the first, it is easy to see that the reachability matrix $R = \left[B_c \; A_c B_c \; \cdots \; A_c^{N-2} B_c \; A_c^{N-1} B_c\right]$ is upper diagonal with nonzero diagonal elements and thereby of full rank. Since the eigenvalues of A_c are all real, the reachability of (9) implies the reachability of the sampled system (10).

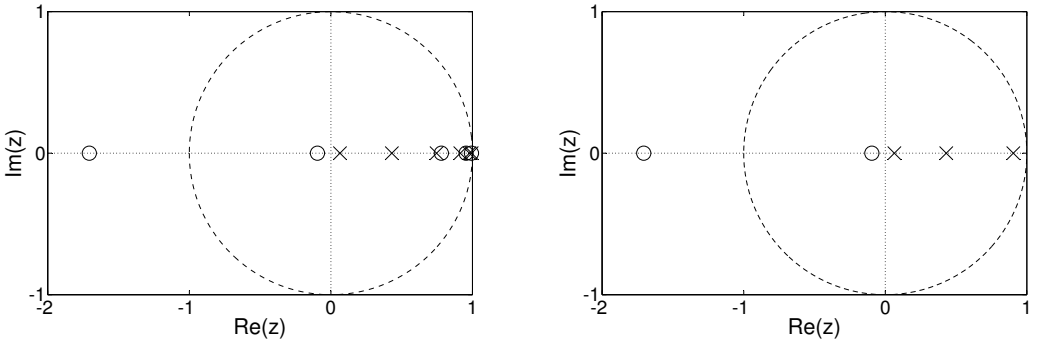

Fig. 3. Pole-zero plots for the open loop (left) and closed loop (right) transfer functions between u and x_m with $N = 6$. Poles are marked with crosses and zeros with circles.

The feedback gain matrix $K \in \mathbb{R}^{1\times N}$ can be calculated (e.g. using Ackermann's formula (Ackermann, 1972)) such that the poles of the closed loop system $A_d - B_d K$ are equal to p_i. In order to have a closed loop steady-state gain of 1, the value of $K_0 \in \mathbb{R}$ is set equal to the inverse of the steady state gain of the closed loop system:

$$K_0^{-1} = C\left(I_N - A_d + B_d K\right)^{-1} B_d \tag{14}$$

with I_N the $N\times N$ identity matrix and $C \in \mathbb{R}^{1\times N}$ containing zeros everywhere except at position m where it is equal to 1.

3.3. PI control

Due to the pole-zero cancellation, the closed loop system with linear state feedback contains m poles p_i and $(m-1)$ sampling zeros τ_i^-. The transfer function of the PI controller is given in the frequency domain by:

$$PI(z) = K_p + \frac{K_i}{z-1} \tag{15}$$

where K_p and K_i are the proportional and integral gains of the controller respectively. This transfer function contains one pole and one zero, so that the resulting closed loop system will contain $(m+1)$ poles and m zeros. The gains K_p and K_i can then be calculated such that the extra zero is canceled with a closed loop pole while the value of the largest pole $p_m = \sigma_m^*$ remains the same.

Integral windup is avoided by multiplying the difference between the control signal and its saturated value with a suitably large gain K_w and feeding it back to the input of the PI controller. A value of $K_w = 0.001\ \mathrm{W^{-1}m}$ was found to be suitable.

4. Numerical results and discussion

The controller developed in the previous section has been evaluated with a number of test case simulations. The simulations were performed with the control structure shown in Figure 2, in which the state space system (A_d, B_d) is replaced by a detailed finite element (FE) model of the thermal dynamics in the workpiece. The used FE model assumes homogeneous material properties in the entire workpiece and contains the additional effects of latent heat and fluid flow in the melt pool driven by Marangoni and buoyancy forces. The effect of material buildup due to the creation of a clad near the tail of the melt pool is ignored. A Gaussian laser intensity profile with a beam diameter of 1.2 mm is used and a constant absorption coefficient of $A = 0.5$ is assumed. The FE simulations were performed with the Argo DGM software using the material parameters for Stainless steel AISI 316L given in Table A.1.

The linear system matrices A_d and B_d were calculated for $N = 9$, $T_{\max} = 2820\ ^\circ\mathrm{C}$ and $u_0 = 400$ W, with a sampling time of $T_s = 1$ ms. The values of $\boldsymbol{x}_0$ are then obtained by solving the system $0 = A_d\boldsymbol{x}_0 + B_d u_0$. The controller gains K, K_0, K_p and K_i were calculated for a desired rise time of $T_r = 10$ ms.

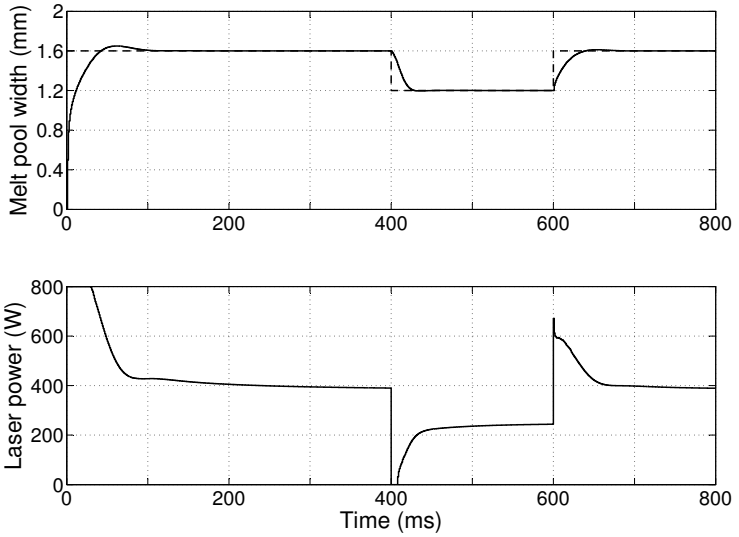

Fig. 4. Simulation results for the heating of a workpiece from ambient temperature with varying reference values (dashed line).

The control system performance is evaluated with a simulation of the heating of a workpiece which is initially at room temperature. At $t = 0$ s the controller is switched on with a reference melt pool width of 1.6 mm (note that this corresponds to setting $x_m^{\text{ref}} = 1.6/2$ mm = 0.8 mm). The maximum laser power is set to 800 W. Figure 4 shows the evolution of the melt pool width over time together with the values of the laser power. From the plots it can be observed that the rise time of the melt pool growth is ca. 10 ms, as expected. A small overshoot of 3% is present, due to the fact that the simulated process is nonlinear and includes unmodeled dynamic effects of latent heat, fluid flow and the use of a Gaussian beam profile. However, thanks to the PI control action a zero steady-state error is quickly reached.

The tracking ability of the controller is illustrated by switching the reference melt pool width to 1.2 mm at $t = 400$ ms and back to 1.6 mm at $t = 600$ ms, as shown in Figure 4. Due to these relatively small step sizes the linearity assumption of the model is a reasonable approximation, which is expressed by the fact that the controller is capable of reaching the lower reference value in ca. 30 ms with an overshoot of only 0.4%. However, the final reference width is reached a bit slower (ca. 40 ms with 0.8% overshoot) which is a clear indication that the model does include a certain degree of nonlinearity.

It was found that the controller is unable to maintain a constant melt pool width smaller than 1.0 mm with the used values for the controller gains. If such low reference values are used, the model needs to be linearized around a lower value of the laser power and the controller gains recalculated.

An important requirement for a controller that is used in the laser cladding process is its robustness with respect to changes in the geometry of the cladded part. The thermal behavior of the melt pool is strongly affected by the shape of the surrounding material: the melting of a solid block of metal is a slow process compared to the rapid heating of the material when building up a thin wall. This can lead to local overheating if no proper action is taken by the controller. Figure 5 illustrates this effect by simulating the growth of the melt pool width when an edge of the workpiece is being approached. If the laser power is kept constant the melt pool grows significantly due to overheating. Activating the controller results in a decrease of the laser power so that a constant melt pool size can successfully be maintained.

5. Conclusions

In this paper a nonlinear heat conduction model for the laser cladding process is presented and linearized for use in the design of a linear state feedback controller. The controller is combined with a PI control law in order to remove a potential steady-state error and improve the disturbance rejection properties. The controller performance is evaluated

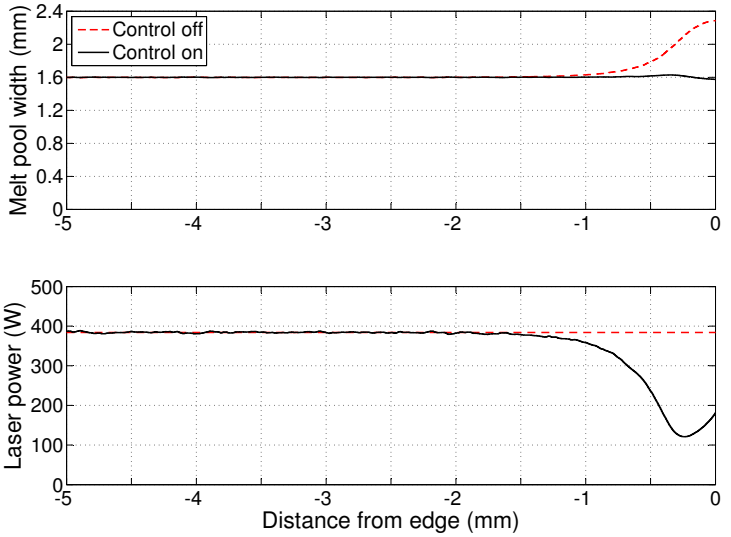

Fig. 5. Simulation results showing the local overheating of the workpiece when approaching an edge without switching on the controller.

with a number of test case simulations which show that a desired constant melt pool size can be maintained with zero steady-state error. The controller is able to track changes in the reference melt pool width with a prescribed speed and can react to changes in geometry of the cladded part.

The presented study indicates that the used heat conduction model can successfully be used to design a linear controller based on temperature feedback, provided that a reliable temperature measurement system is available. In order to correctly asses the practical performance of such a controller, an improved finite element model including the material buildup due to the creation of a clad needs to be used when numerically testing the control system. Furthermore, a practical implementation of the controller, which is currently being prepared by the authors, is required to validate the real-life performance.

Acknowledgements

This work was supported by the Agency for Innovation by Science and Technology in Flanders (IWT) within the SBO 110070 eSHM with AM project, and the Research Council (OZR) of the Vrije Universiteit Brussel. The authors would like to thank the Argo team at Cenaero, Jean-Sébastien Cagnone and Koen Hillewaert in particular, for their continuous support with the use of the software.

Appendix A. Model parameters

Table A.1. Model parameters used in simulations (Lide, 2010; Brandes and Brook, 1992).

Parameter	Symbol	Value	Unit
Specific heat	C_p	500	J/(kg·K)
Latent heat of fusion	Δh	270	kJ/kg
Thermal conductivity	k	20	W/(m·K)
Ambient temperature	T_0	20	°C
Melting temperature	T_m	1420	°C
Laser speed	U	6.67	mm/s
Thermal expansion coefficient	β	$1.96 \cdot 10^{-5}$	K^{-1}
Dynamic viscosity	μ	$6 \cdot 10^{-3}$	kg/(m·s)
Density	ρ	7990	kg/m^3

References

Ackermann, J., 1972. Der Entwurf linearer Regelungssysteme im Zustandraum. Regelungstechnik und Prozess-Datenverarbeitung 7, 297-300.

Bi, G., Gasser, A., Wissenbach, K., Drenker, A., Poprawe, R., 2006. Characterization of the process control for the direct laser metallic powder deposition. Surface & Coatings Technology 201, 2676-2683.

Brandes, E.A., Brook, G.B., 1992. Smithells Metals Reference Book, 7th ed. Butterworth-Heinemann, Oxford.

Devesse, W., De Baere, D., Guillaume, P., 2014. The isotherm migration method in spherical coordinates with a moving heat source. International Journal of Heat and Mass Transfer 75, 726-735.

Doumanidis, C., Kwak, Y.-M., 2001. Geometry modeling and control by infrared and laser sensing in thermal manufacturing with material deposition. Journal of Manufacturing Science and Engineering 123, 45-52.

Dowden, J.M., 2001. The Mathematics of Thermal Modeling: An Introduction to the Theory of Laser Material Processing. CRC Press, Boca Raton.

Fathi, A., Khajepour, A., Toyserkani, E., Durali, M., 2007. Clad height control in laser solid freeform fabrication using a feedforward PID controller. International Journal of Advanced Manufacturing Technology 35, 280-292.

Hofman, J.T., Pathiraj, B., van Dijk, J., de Lange, D.F., Meijer, J., 2012. A camera based feedback control strategy for the laser cladding process. Journal of Materials Processing Technology 212, 2455-2462.

Lide, D.R., 2010. CRC Handbook of Chemistry and Physics, 90th ed. CRC Press, Boca Raton.

Rosenthal, D., 1946. The theory of moving source of heat and its application to metal treatment. Transactions of the ASME 43, 849-866.

Salehi, D., Brandt, M., 2006. Melt pool temperature control using LabVIEW in Nd:YAG laser blown powder cladding process. International Journal of Advanced Manufacturing Technology 29, 273-278.

Song, L., Bagavath-Singh, V., Dutta, B., Mazumder, J., 2012. Control of melt pool temperature and deposition height during direct metal deposition process. International Journal of Advanced Manufacturing Technology 58, 247-256.

Toyserkani, E., Khajepour, A., Corbin, S., 2005. Laser Cladding. CRC Press, Boca Raton.